Microstructural and fractographic analysis of non-equiatomic alloy of Co – Cr – Fe – Mn – Ni system

V. K. Drobyshev, *Researcher, Laboratory of Electron Microscopy and Image Processing*[1], *e-mail: drobyshev_v.k@mail.ru*
S. V. Konovalov, *Professor, Doctor of Technical Sciences, Vice-Rector for Research and Innovation*[1], *e-mail: konovalov@sibsiu.ru*
I. A. Panchenko, *Candidate of Technical Sciences, Head of the Laboratory of Electron Microscopy and Image Processing*[1], *e-mail: i.r.i.ss@yandex.ru*

[1] *Siberian State Industrial University, Novokuznetsk, Russia.*

In the present work, the microstructure of $Co_{20}Cr_{20}Fe_{10}Mn_{30}Ni_{20}$ high-entropy alloy with increased Mn content and decreased Fe content, which was obtained by vacuum induction melting, was studied. The study evaluates the effect of Fe and Mn content percentages on the microstructure and mechanical properties of high entropy alloy (HEA). The relationship between the microstructure (formation of solid solution phases) and mechanical properties of HEA in comparison with the high-entropy equiatomic Cantor alloy is investigated. Studies of the structure, phase and chemical composition of the material were obtained using *X*-ray diffraction and scanning electron microscopy. It is shown that the studied alloy is a material consisting of a single-phase solid solution with a face-centered cubic lattice and a structure represented in the form of dendrite branches of the first, second and third order. Energy dispersive *X*-ray spectroscopy revealed that the dendrite axes are enriched with chromium, iron and cobalt atoms, while manganese and nickel predominate in the interdendritic areas. It is likely that during crystallization process, such elements as manganese and nickel have time to be redistributed and released in the form of second-phase particles in the interaxial spaces of dendrites. Destruction of the material is represented by ductile fracture with the content of deep fracture holes, indicating high plasticity of the material, as well as the presence of globular oxide inclusions, which are more enriched in manganese, oxygen and chromium atoms.
According to the conducted tensile tests, it was found that the samples of $Co_{20}Cr_{20}Fe_{10}Mn_{30}Ni_{20}$ mainly have high (more than 80%) plasticity and $\sigma_{0.2}$ = 236 MPa, σ_{lim} = 478 MPa, respectively. The result also shows that the decrease of Fe and increase of Mn in the alloy increases the strain hardening rate, which further increases the embrittlement degree. It is found that the composition of the area containing non-metallic inclusion in $Co_{20}Cr_{20}Fe_{10}Mn_{30}Ni_{20}$ alloy is more enriched in manganese, oxygen and chromium.

Key words: scanning electron microscopy, high entropy alloy, structure, ductile fracture, element mapping, non-metallic inclusions.

DOI: 10.17580/nfm.2024.02.10

Introduction

The traditional approach in the creation of structural materials is to select a basic element as a matrix to obtain the desired combination of mechanical properties. A large number of alloys used in practice have been obtained, based on iron, copper, aluminum, and others. For the last two decades, the approach to the creation of multicomponent alloys having 5 or more elements in equal equiatomic proportions as a matrix has been very interesting [1–5]. A new class of materials, called high-entropy alloys (HEAs), as noted in [6], has an almost limitless number of alloys, which was successfully demonstrated in Ref. [7, 8]. Among various alloys, an equiatomic alloy containing Co, Cr, Fe, Mn and Ni (high entropy Cantor alloy) with face-centered cubic phase is becoming increasingly popular due to its excellent mechanical properties [9, 10]. The use of equiatomic CoCrFeMnNi alloy can significantly increase equipment life and durability due to its exceptional strength, ductility and fracture toughness [11, 12]. A number of closely related or non-equiatomic high-entropy alloys have been developed that have been found to be stronger and more ductile than their predecessors [13]. Compared to high-entropy alloys, commonly used structural materials such as steels, nickel and other alloys are known to have a negative effect on the corrosion and mechanical properties of the material [14]. Conventional melting technologies are therefore often unsuitable. Vacuum induction melting, vacuum arc remelting and electroslag melting are the main technologies used to produce high-entropy alloys. Among these, the vacuum induction melting process offers the opportunity to limit the presence of hydrogen, oxygen and nitrogen in the melt.

The works on high-entropy alloys presented by the authors [15, 16] emphasize the study of the influence of one component at a proportional change in the content of other components, but for further search for alloys with new properties it is necessary to expand the field of study to the simultaneous influence of two or more components.

In the present work, the microstrцucture of $Co_{20}Cr_{20}Fe_{10}Mn_{30}Ni_{20}$ high-entropy alloy with increased Mn content and decreased Fe content obtained by vacuum

induction melting is studied. The present study evaluates the effect of Fe and Mn percentage on the microstructure and mechanical properties of the high-entropy alloy. The relationship between the microstructure (formation of solid solution phases) and mechanical properties of HEA was investigated in comparison with the high-entropy equiatomic Cantor alloy.

Materials and methods

The $Co_{20}Cr_{20}Fe_{10}Mn_{30}Ni_{20}$ alloy was chosen as the object of the study; its production was carried out by closed technology in production conditions by the "TSM" LLC R&D Center supplier company in a vacuum induction furnace VIP-010 in a corundum crucible with a capacity of 10 kg. As initial charge materials for smelting were used branded pure charge materials, presented in **Table 1.**

Samples were cut out of the obtained ingot (**Fig. 1**) on a DK7732 M11 jet-type electric discharge machine for further studies of phase, elemental composition and mechanical tests. In order to obtain a high-quality surface of the microslice for studies by scanning electron microscopy (SEM) and *X*-ray phase analysis (XRF), the grinding process was successively passed from one abrasive skin to another with continuously decreasing sizes of abrasive particles and further polishing of the sample using a special cloth and paste. To reveal the microstructure of the $Co_{20}Cr_{20}Fe_{10}Mn_{30}Ni_{20}$ composition sample, etching was carried out in a reagent consisting of HNO_3 and HCl in the ratio of 1 : 3, etching time was 30 s. Tensile tests were carried out on flat proportional samples in the form of double-sided blades with the size, in accordance with GOST1497–84.

The deformation was performed by uniaxial tension of 5 specimens on a UBRAMAX PM BC-50-A-1-02-II machine at a test speed of 2 mm/min. The structure and elemental composition of the samples were studied by scanning electron microscopy (KYKY EM-6900 instrument equipped with Oxford Xplore energy dispersive analyzer) with an accelerating voltage of 30 kV, a filament current of 2.20 A and an emission current of 150-10-6 A. Averaging of elemental composition using energy dispersive *X*-ray spectroscopy was carried out for 5 points. *X*-ray diffractometer Shimadzu XRD-6000 was used for *X*-ray phase analysis; imaging was carried out in copper filtered radiation Cu-$K\alpha$1. PDF 4+ databases and POWDER CELL 2.4 full-profile analysis programs were used to analyze the phase composition. To predict the phase composition, we used the program HEApredict_v.1, developed by the members of the research team, which allows us to calculate thermodynamic and phenomenological parameters of a high-entropy alloy and, based on the criteria known from the literature, to predict the phase composition.

Table 1
Brand and list of valid standards for the materials used

Element	Brand	Degree of purity, %	Regulatory document
Chromium	ЭХМД-ULTRA	>99.90	TU 24145.30.220-16-05762312–2017
Cobalt	К1Ау	>99.90	GOST 123–2018
Ferrum	АРМКО ТИП-1	>99.90	GOST 2591–88, TU 00187895-103–2019
Nickel	ДНК-0	>99.90	GOST 849–2018
Manganese	Мн998	99.98	GOST 6008–90

Fig. 1. $Co_{20}Cr_{20}Fe_{10}Mn_{30}Ni_{20}$ alloy ingot and specimen size for uniaxial tensile testing

Results and Discussion

Fig. 2 and **Table 2** show the *X*-ray diffraction pattern of the sample and lattice parameters of the high-entropy alloy. The investigated alloy, demonstrate one face-centered cubic (FCC) phase, which is confirmed by distinct diffraction peaks for crystallographic planes (111), (200) and (220) with an average crystallite size of 202.6 Å The diffraction pattern shows only the peaks of the FCC phase.

Based on the prediction of the phase composition of the high-entropy alloy in **Table 3**, it was found that at a manganese content ≥30%, a sigma phase is formed in the alloy. By the method of SEM analysis, conclusions were made about the formation of eutectic reaction in the interdendritic areas with the formation of a mixture of phases. Thus, based on the results of [17], it can be stated that the change in the content of components near the initial equiatomic alloy, affects the chemical, phase composition of the alloy and the dendrite growth process.

To evaluate the alloy structure, electron microscopic images of the structure of the $Co_{20}Cr_{20}Fe_{10}Mn_{30}Ni_{20}$ alloy are shown in **Fig. 3**. It can be noted that this alloy consists of a single-phase solid solution with a FCC lattice with a structure represented in the form of dendrite branches (**Fig. 3, *b***).

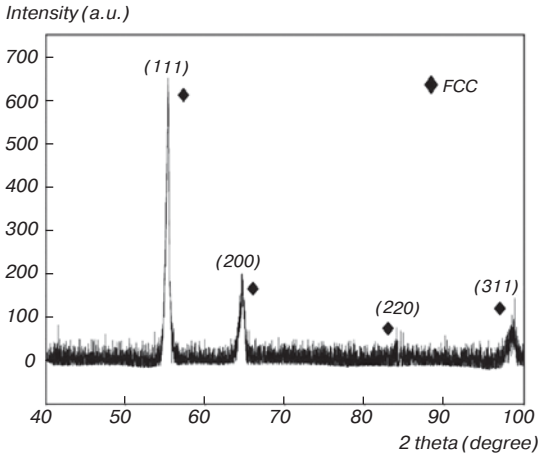

Fig. 2. *X*-ray diagram of the $Co_{20}Cr_{20}Fe_{10}Mn_{30}Ni_{20}$ alloy

Table 2
Lattice parameters at different values of the crystallographic plane

Crystallographic planes	Parameter ***a*** of the lattice, Å	Crystallite size, Å
111	2.08	133.835
200	1.80	227.109
220	1.27	247.161
Average value	1.72	1.72

The microstructure of the investigated sample is basically dense and homogeneous. When comparing the SEM image of $Co_{20}Cr_{20}Fe_{10}Mn_{30}Ni_{20}$ alloy with $Co_{20}Cr_{20}Fe_{10}Mn_{20}Mn_{20}Ni_{20}$ alloy presented in [18], obtained by vacuum-arc melting, the microstructure of $Co_{20}Cr_{20}Fe_{10}Mn_{30}Ni_{20}$ alloy has dense and homogeneous dendritic and interdendritic areas.

Fig. 4, ***a*** shows the SEM morphology of $Co_{20}Cr_{20}Fe_{10}Mn_{30}Ni_{20}$ alloy. A large number of dendritic phases were observed in the sample. Thus it can be concluded that the presence of interdendritic phase is more prominent with increasing percentage of Mn content. As a result, there is a growth of intermetallic phases due to the consumption of solid solution phases.

The energy spectra presented in **Fig. 4** indicate that manganese, iron, nickel, chromium and cobalt atoms are present in the investigated material. The results of the averaged quantitative analysis of the chemical composition of the $Co_{20}Cr_{20}Fe_{10}Mn_{30}Ni_{20}$ alloy revealed that the main elements are Co ((19.21 ± 0.26) at.%), Cr ((19.82 ± 0.33) at.%), Fe ((9.69 ± 0.04) at.%), Mn ((32.26 ± 0.35) at.%) and Ni ((19.96 ± 0.02) at.%))).

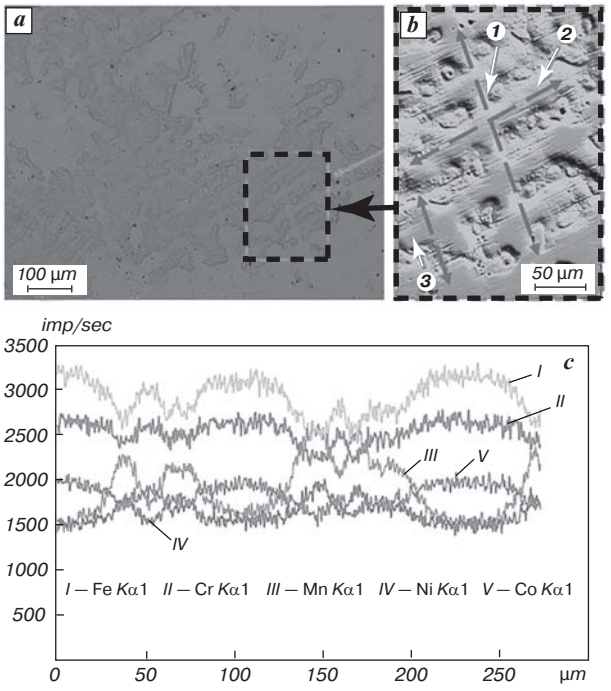

Fig. 3. Electron microscopic image of the $Co_{20}Cr_{20}Fe_{10}Mn_{30}Ni_{20}$ high-entropy alloy structure film surface after three cycles of modification at magnification: ×100 (*a*), ×1000 (*b*), where *1*, *2*, *3* are the first, second and third order axes, (*c*) micro-*X*-ray spectral analysis along the line

The method of scanning electron microscopy (**Fig. 4**) revealed the distribution of chemical elements content in the dendritic areas of the investigated section of HEA. This was also revealed in the micro-*X*-ray spectral analysis of the surface layer of the sample by the "along the line" method presented in **Fig. 3,** ***c***. Heterogeneous distribution of chemical elements in the axes and interaxial spaces of dendrites (dendritic liquation): Cr, Co, Fe are concentrated in the dendrite axes, Mn and Ni stand out along the boundaries, prevailing in the interdendritic areas. It is likely that during the crystallization process, such elements as manganese and nickel have time to be redistributed and released in the form of second-phase particles in the interaxial spaces of dendrites. This is also indicated by the results of quantitative elemental analysis presented in **Table 4**.

A characteristic view of the tensile strain curve of high-entropy alloys of the $Co_{20}Cr_{20}Fe_{10}Mn_{30}Ni_{20}$ system in the cast state is shown in **Fig. 5**. The samples have high (> 80 %) plasticity and tensile strength of 478 ± 14 MPa.

Table 3
Prediction of phase composition of high-entropy alloys of Co – Cr – Fe – Mn – Ni system at change of Fe and Mn content

Alloy	Solid solution	BCC	FCC	BCC +FCC	TCP	σ-phase in alloys, with Cr and/or V
$CoCrFe_xMnNi$	$0 \le x < 100$ at. %.	–	$20 \le x < 100$ at. %.	–	$0 \le x < 30$ at. %.	–
$CoCrFeMn_xNi$	$0 \le x < 100$ at. %.	–	$0 \le x < 10$ at. %.	$40 \le x < 100$ at. %.	$20 \le x < 60$ at. %.	$30 \le x < 100$ at. %

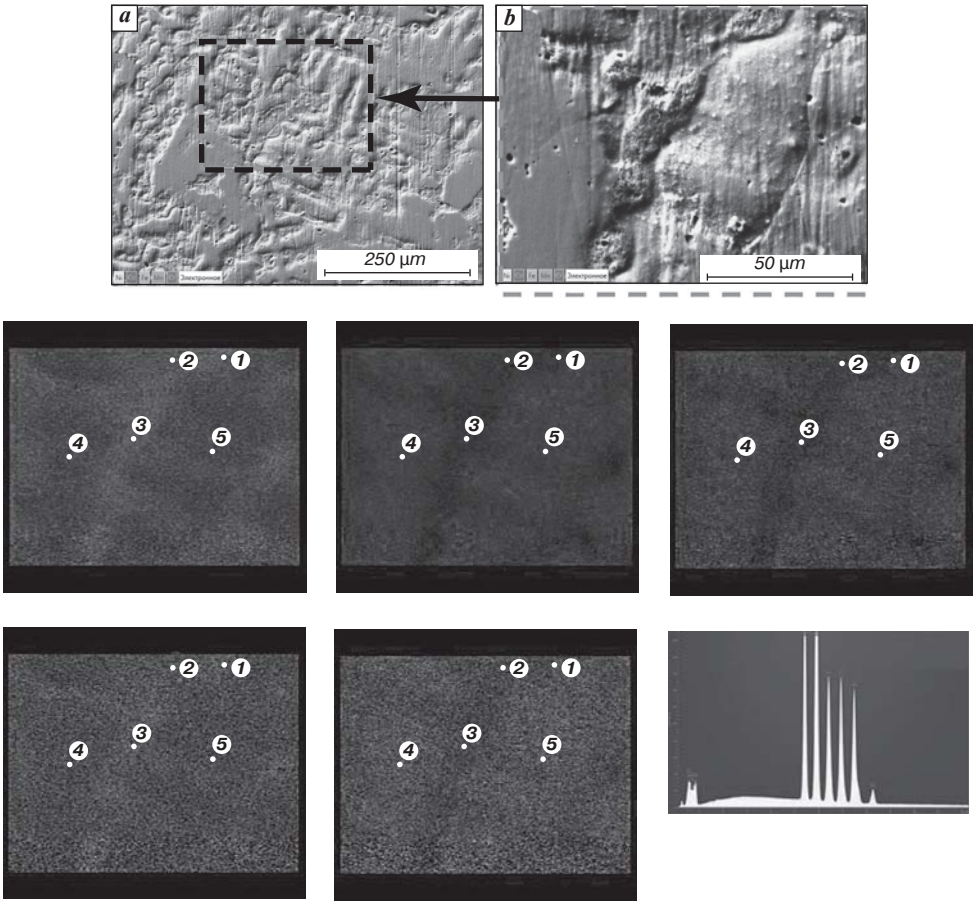

Fig. 4. Electron microscopic image of the HEA surface structure and elemental mapping of the dendritic and interdendritic area: ×500 (*a*), ×2000 (*b*)

Table 4
The results of the micro-*X*-ray spectral analysis of the HEA presented in Fig. 2

Element, at. %	Cr	Mn	Fe	Co	Ni
Spectrum 1 (interdendritic area)	12.41	43.41	5.34	13.85	25.00
Spectrum 2 (interdendritic area)	16.28	37.92	7.65	17.69	20.47
Spectrum 3 (interdendritic area)	14.20	40.20	6.56	15.32	23.71
Spectrum 4 (dendritic area)	21.74	28.59	11.12	21.32	17.24
Spectrum 5 (dendritic area)	22.89	27.81	11.77	21.58	15.95
Average	16.16	37.53	7.67	17.05	21.06

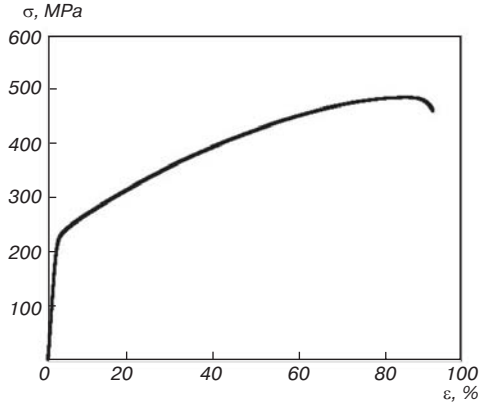

Fig. 5. Characteristic strain curve of $Co_{20}Cr_{20}Fe_{10}Mn_{30}Ni_{20}$ alloy

Table 5 shows a comparative analysis of mechanical properties of Co – Cr – Fe – Mn – Ni HEA. The revealed significant discrepancies may be due to the shape and size of samples, method of their obtaining, testing modes. The decrease in tensile strength may be due to the formation of defects during casting, such as pores and microcracks, which become sources of cracking when the material fails. Under external load, multiple sources of cracking will expand and connect until the entire material collapses. Factors such as the coefficient of thermal expansion and the mismatch of elastic moduli between the reinforcing phases and the matrix play a role in tensile properties. The released phase is distributed around the grains and is mainly responsible for the elastic modulus. The result also shows that decreasing Fe and increasing Mn in the alloy increases the strain hardening rate, which further increases the degree of embrittlement. The increase in strain hardening can lead to an increase in microcracks, thereby contributing to material destruction.

SEM-images of the surface after tensile testing are shown on **Figs. 6–7**. The surface after tensile testing of the studied alloy is represented by a ductile fracture **(Fig. 6, *a, c, d*)** with the content of deep fracture holes, indicating high plasticity of the material.

The performed micrographs of the fracture surface of the high-entropy alloy for counting the number and size of holes are presented in **Fig. 6, *b***. Analyzing this information, we can note the presence of equiaxed holes up to 5 μm in size with globular inclusions with a diameter

Table 5
Mechanical properties of high-entropy alloys of Co – Cr – Fe – Mn – Ni system after uniaxial tensile tests

	$\sigma_{0.2}$, MPa	σ_{lim}, MPa	Tensile elongation
Present work	236	478 ± 14	86
Cast state [19]	–	494	–
Cast state [20]	230	–	62

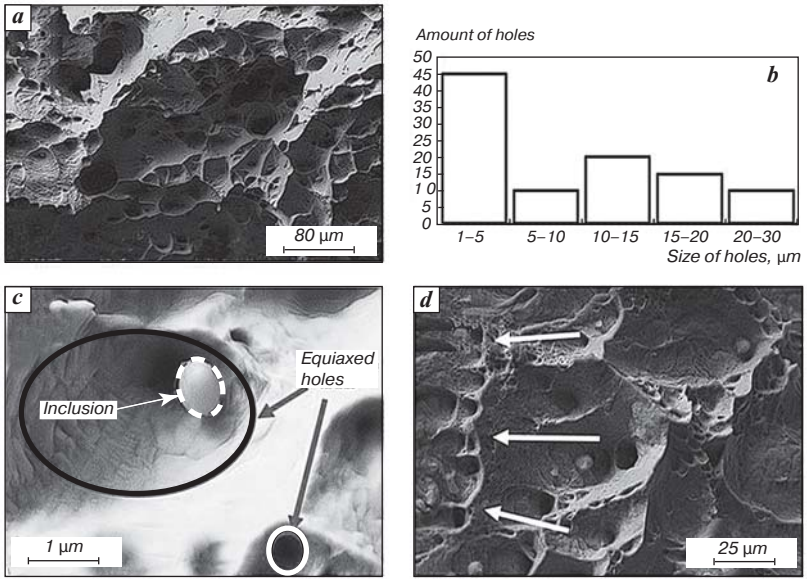

Fig. 6. SEM images of the fracture surface of $Co_{20}Cr_{20}Fe_{10}Mn_{30}Ni_{20}$ high-entropy alloy: *a* — macrophotograph of ductile fracture of high-entropy alloy, *b* — plot of hole size distribution, *c* — image containing non-metallic inclusion and equiaxed holes, *d* — electron microscopic image containing shear holes and their direction

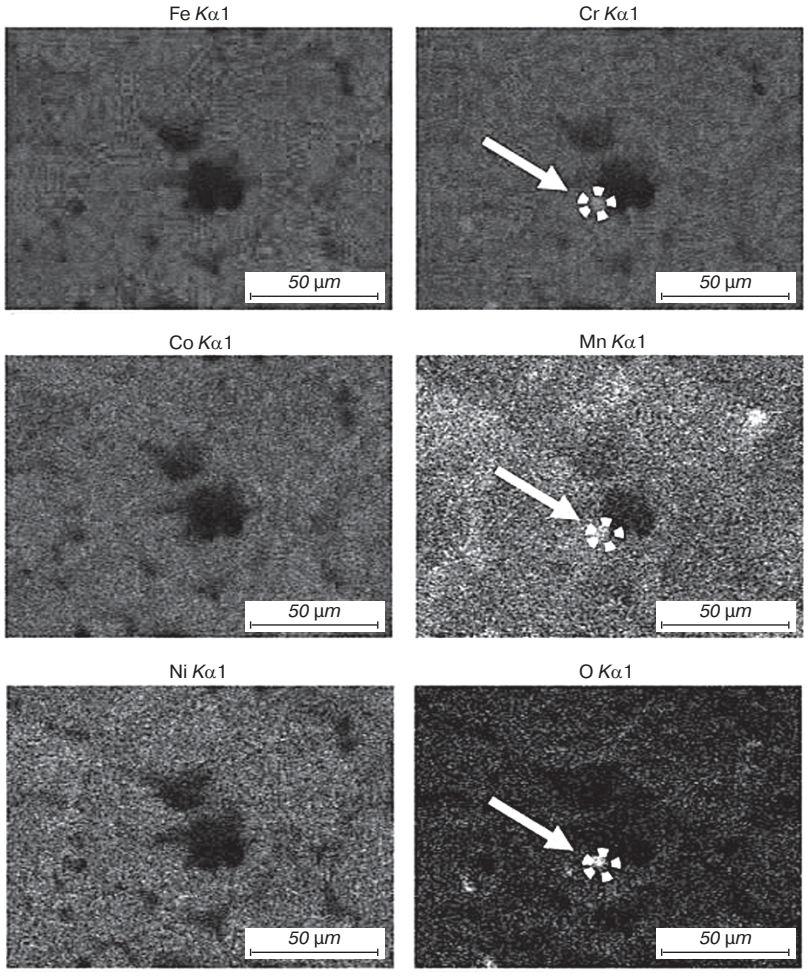

Fig. 7. EMF analysis of $Co_{20}Cr_{20}Fe_{10}Mn_{30}Ni_{20}$ alloy after stretching, which contains globular inclusions

of 6 ± 1 μm and the presence of different types of holes (equiaxed and shear holes) presented in **Fig. 6**. The largest size of equiaxial holes is 20–30 μm from clowholes in the interaxial spaces. Due to the casting process, extremely small pores (**Fig. 6, *b***) and other defects are formed in the material. Under the action of external load, microcracks preferentially arise from these pores, gradually expand, leading to the formation of crack sources of the "rupture" first type cracks. In addition, due to the difference in plasticity of hard phases containing Mn and Ni and soft phases, stress concentration phenomenon occurs at weak interfacial bonding, leading to the formation and growth of micropores.

An elemental mapping method was conducted to evaluate the distribution of each element investigated by the HEA after the tensile test. Secondary precipitates with irregular shape were observed (**Fig. 7**). The results showed the formation of Cr oxides and carbides. The uneven distribution of Cr was relatively characteristic of the cast alloy (**Fig. 7**). Cr carbides present in CoCrFeMnNi alloy were identified as $Cr_{23}C_6$ and Cr_7C. The composition of the region containing the non-metallic inclusion in the $Co_{20}Cr_{20}Fe_{10}Mn_{30}Ni_{20}$ alloy was found to be more enriched in manganese, oxygen and chromium.

Conclusion

In the present work, the $Co_{20}Cr_{20}Fe_{10}Mn_{30}Ni_{20}$ high-entropy alloy is investigated. It is a material with a structure represented in the form of dendrite branches, the grain volume of which is predominated by chromium, cobalt, iron, and in the boundary regions by manganese and nickel. The microstructure of the $Co_{20}Cr_{20}Fe_{10}Mn_{30}Ni_{20}$ alloy has dense homogeneous dendritic and interdendritic areas. The high value of tensile strength 478 ± 14 MPa of the investigated alloy is due to the presence of intermetallic compounds in the alloy, which leads to hardening of the secondary phase. However, due to the significant difference in plasticity between hard phases containing Mn and Ni and soft phases, stress concentration occurs at weak interfacial bonds. Destruction of the material is represented by ductile fracture with the content of deep fracture holes, indicating high plasticity of the material, as well as the presence of globular

oxide inclusions, which are more enriched in manganese, oxygen and chromium atoms.

The study was funded by the Russian Science Foundation grant No. 23-49-00015, https://rscf.ru/project/23-49-00015/.

References

1. Murty B. S., Yeh J. W., Ranganathan S. High-Entropy Alloys. Butterworth-Heinemann (Elsevier), 2014. 218 p.

2. Tsai K.-Y., Tsai M.-H., Yeh J.-W. Sluggish Diffusion in Co – Cr – Fe – Mn – Ni High-Entropy Alloys. *Acta Materialia*. 2013. Vol. 61, Iss. 13. pp. 4887–4897.

3. Isali A., George E. P. Tensile Properties of High- and Medium-Entropy Alloys. *Intermetallics*. 2013. Vol. 39. pp. 74–78.

4. Wang Z., Baker I., Guo W., Poplawsky J. D. The Effect of Carbon on the Micro-Structures, Mechanical Properties, and Deformation Mechanisms of Thermo-Mechanically Treated $Fe_{40.4}Ni_{11.3}Mn_{34.8}Al_{7.5}Cr_6$ High Entropy Alloys. *Acta Materialia*. 2017. Vol. 126. pp. 346–360.

5. Li Z. Interstitial Equiatomic CoCrFeMnNi High-Entropy Alloys: Carbon Content, Microstructure, and Compositional Homogeneity Effects on Deformation Behavior. *Acta Materialia*. 2019. Vol. 164. pp. 400–412.

6. Lukianova O. A., Rao Z., Kulitskii V., Li Z., Wilde G., Divinski S. V. Impact of Interstitial Carbon on Self-Diffusion in CoCrFeMnNi High Entropy Alloys. *Scripta Materialia*. 2020. Vol. 188. P. 264–268.

7. Stepanov N. D., Shaysultanov D. G., Chernichenko R. S., Yurchenko N. Yu., Zherebtsov S. V., Tikhonovsky M. A., Salishchev G. A. Effect of Thermomechanical Processing on Microstructure and Mechanical Properties of the Carbon-Containing CoCrFeNiMn High Entropy Alloy. *Journal of Alloys and Compounds*. 2017. Vol. 693. pp. 394–405.

8. Easo P. G., Dierk R., Robert O. R. High-Entropy Alloys. *Nature Reviews Materials*. 2019. Vol. 4. pp. 515–534.

9. Cantor B., Chang I. T. H., Knight P., Vincent A. J. B. Microstructural Development in Equiatomic Multicomponent Alloys. *Materials Science and Engineering: A*. 2004. Vol. 375–377. pp. 213–218.

10. Galano M., Audebert F., Cantor B., Stone I. Structural Characterisation and Stability of New Nanoquasicrystalline Al-Based Alloys. *Materials Science and Engineering: A*. 2004. Vol. 375–377. pp. 1206–1211.

11. Shahmir H., Mehranpour M. S., Shams S. A. A., Langdon T. G. Twenty Years of the CoCrFeNiMn High-Entropy Alloy: Achieving Exceptional Mechanical Properties Through Microstructure Engineering. *Journal of Materials Research and Technology*. 2023. Vol. 23. pp. 3362–3423.

12. Yang K., Huang Q., Zhong B., Liu Y. J., He C., Liu H., Su N., Wang Q., Chen Q. Influence of the Volume Content of $\alpha + \beta$ Colonies on the Very High Cycle Fatigue Behavior of a Titanium Alloy. *Fatigue & Fracture of Engineering Materials & Structures*. 2021. Vol. 44, Iss. 10. pp. 2643–2658.

13. Stepanov N., Shaysultanov D., Klimova M., Sanin V., Zherebtsov S. Strengthening of a CoCrFeNiMn-Type High Entropy Alloy by Regular Arrays of Nanoprecipitates. *Materials Science Forum*. 2018. Vol. 941. pp. 772–777.

14. Wei D., Gong W., Kawasaki T., Harjo S., Kato H. Regulation of Strength and Ductility of Single-Phase Twinning-Induced Plasticity High-Entropy Alloys. *Scripta Materialia*. 2022. Vol. 216. 114738.

15. Wan T., Huang Z., Cheng Z., Zhu M., Zhu W., Li Z., Fu D., Ren F. The Effect of Chromium Content on the Corrosion Behavior of Ultrafine-Grained Cr_xMnFeCoNi High-Entropy Alloys in Sulfuric Acid Solution. *Microstructures*. 2023. Vol. 3. 2023014.

16. Liu Y., Liu W., Zhou Q.-Y., Liu C., Fan T.-W., Wu Y.-Z., Wang Z.-P., Tang P.-Y. An Initio Study of Thermodynamic and Fracture Properties of CrFeCoNiMnx ($0 \le x \le 3$) High-Entropy Alloys. *Journal of Materials Research and Technology*. 2022. Vol. 17. pp. 498–506.

17. Tung C.-C., Yeh J.-W., Shun T.-T., Chen S.-K., Huang Y.-S., Chen H.-C. On the Elemental Effect of AlCoCrCuFeNi High-Entropy Alloy System. *Materials Letters*. 2007. Vol. 61, Iss. 1. pp. 1–5.

18. Karantzalis A. E., Poulia A., Kamnis S., Sfikas A., Fotsis A., Georgatis E. Modification of Cantor High Entropy Alloy by the Addition of Mo and Nb: Microstructure Evaluation, Nanoindentation-Based Mechanical Properties, and Sliding Wear Response Assessment. *Alloys* 2022. Vol. 1, Iss. 1. pp. 70–92.

19. Otto F., Dlouhý A., Somsen Ch., Bei H., Eggeler G., George E. P. The Influences of Temperature and Microstructure on the Tensile Properties of a CoCrFeMnNi Highentropy Alloy. *Acta Materialia*. 2013. Vol. 61, Iss. 5. pp. 5743–5755.

20. Stepanov N. D., Shaysultanov D. G., Salishchev G. A., Tikhonovsky M. A., Oleynik E. E., Tortika A. S., Senkov O. N. Effect of V Content on Microstructure and Mechanical Properties of the CoCrFeMnNiV_x High Entropy Alloys. *Journal of Alloys and Compounds*. 2015. Vol. 628. pp. 170–185.